Exciton mixing in quantum wells

Gerrit E. W. Bauer
Philips Research Laboratories, Post Box 80 000, NL-5600 JA Eindhoven, The Netherlands

Tsuneya Ando
Institute for Solid State Physics, University of Tokyo, 7-22-1 Roppongi, Minato-ku, Tokyo 106, Japan
(Received 4 April 1988)

An effective-mass theory of the properties of excitons in isolated GaAs/$Al_xGa_{1-x}As$ quantum wells is presented. The phenomenon of exciton mixing induced by the complicated valence-band structure is emphasized. The effects of external perturbations such as electric and magnetic fields and uniaxial pressure normal to quantum wells grown in different crystal directions are calculated. Exciton mixing is found to cause many observable effects on transition energies and oscillator strengths.

I. INTRODUCTION

Since the pioneering work of Dingle,[1] excitons in semiconductor quantum wells have been subject to numerous studies motivated by the pronounced effects of quasi-two-dimensionality in the excitonic features of optical spectra. The quantities of interest are energies and oscillator strengths of the optical transitions associated with the creation or annihilation of an exciton state.

Experimentally, excitons at the direct band gap of intrinsic GaAs/$Al_xGa_{1-x}As$ quantum wells have been studied extensively by absorption, excitation, photoluminescence, photoconductivity, and reflectance spectroscopy,[1-28] where the list of references is by no means exhaustive. Of special interest are the exciton properties in the presence of external perturbations. Characteristic effects of magnetic[8-15] and electric fields,[16-21] or both,[22] and externally applied pressure[18,23,24] have been reported. The effect of crystal orientation of the quantum well on the properties of excitons has been examined in Ref. 25. Many experimental results show clear effects of exciton mixing like exciton transitions which are forbidden in a simple two-band model[5,25] or anticrossing behavior of excited exciton states.[19,21,22,24] Two-photon magneto-optical spectroscopy on quantum wells[26] provides information on exciton states which are parity forbidden in conventional optical experiments.

A large number of theoretical studies of the problem have been published as well. The simplest model of a (type-I) quantum-well exciton is an electron and a hole moving in a common plane exhibiting a binding energy enhanced by a factor of 4 compared with the bulk system.[29,30] The effect of the finite well width has been investigated by Miller *et al.*[2] and others[31,32,6] using a model in which an electron-hole pair is confined between two parallel, infinitely high potential barriers. The additional spatial degree of freedom decreases the exciton binding energy. Tunneling of the exciton into finite potential barriers leads to a further reduction of the binding energy.[33-35] Effects of external electric and magnetic fields have also been extensively investigated[13,20,36-43] using the above-mentioned simple models. All these early studies disregarded the complications introduced by the valence-band degeneracy of GaAs. But, as illustrated by numerous band-structure calculations for valence-band holes in quantum wells, see e.g., Refs. 44 and 45 and Fig. 3, the light and heavy holes couple rather strongly, and significant effects on the excitons may be expected.

Considerable experience has been accumulated with regard to the treatment of valence-band mixing effects on magnetoexcitons in bulk semiconductors by effective-mass theory.[46-50] Methods which are valid for very weak and very strong magnetic fields[46-48] have been superseded by the work of Lipari and Altarelli[49,50] in which the exciton envelope function is expanded into spherical tensors, which allows an analytical evaluation of the angular integrals in the Hamiltonian matrix elements. With use of a nonorthogonal basis for the radial functions, high numerical accuracy has been achieved for the ground-state excitons.[49,50] The spirit of the present study is similar to that of Ref. 49, but the presence of a quantum-well potential increases the complexity of the problem considerably.

Recently, a number of calculations of the effects of valence-band mixing on excitons in quantum wells have been reported.[51-59] Sanders and Chang[51] tackled the problem by expanding the exciton envelope function into products of the wave-vector-dependent electron and hole quantum-well envelope functions, where the latter are already mixed. The secular equation is then solved in momentum space. A similar approach has been chosen by Broido and Sham,[52] who also estimate the effect of the resonance coupling of the light-hole exciton ground state with the heavy-hole exciton continuum. Chan[53] on the other hand has calculated binding energies by a real-space approach which is similar to ours, though he used a limited basis set. Ekenberg and Altarelli[54] present a perturbation-theoretical study on exciton binding energies and a critical comparison with other work. The calculations in Refs. 51 and 52 have been recently criticized[55-57] to neglect the proper angular momentum character of the exciton envelope functions. The discrepan-

cies between results from different theories noted in Ref. 54 can apparently be explained by the corresponding overestimation of exciton binding energies.

A few studies aim at a simultaneous treatment of valence-band mixing and external perturbations. Using the method of Ref. 51 mentioned above, Sanders and Chang[58] calculated the effects of uniaxial pressure along the growth direction and Sanders and Bajaj[59] the effects of electric fields and band-gap grading normal to the quantum well. In the latter work exciton spin splittings are found which are unphysical because Kramer's degeneracy is not broken by electric fields. Pressure effects have been discussed by Hiroshima[60] but under provision of simplifications like a spherically symmetric kinetic energy operator for the holes. Excitons in quantum wells subject to high magnetic fields have been studied by Yang and Sham.[61] Their theory is quoted to be valid for magnetic fields stronger than 6 tesla, and is in this sense complementary to ours, which is designed for weak and intermediate fields up to 10 tesla. They carry out calculations for a few magnetic fields only and claim a numerical accuracy of about 10%. At high magnetic fields and/or at high energies the mixings due to the Coulomb interaction should be less important and magnetooptical spectra appear to also be well explained by calculations of the Landau-level transitions which are *a posteriori* corrected for excitonic effects.[62,63] Finally the work of Masselink *et al.*[64] on the related problem of shallow acceptor states in quantum wells should be referred to.

Here we consider direct-gap quantum wells grown in the main crystal directions [001], [110], and [111]. We present numerical results of the properties of excitons obtained in an effective-mass type of approximation. The Luttinger Hamiltonian[65] is used to describe the hybridization of light- and heavy-hole bands. Electric and magnetic fields and stress normal to the interfaces are treated simultaneously. In intermediate magnetic fields we may not resort to perturbation theory or to the neglect of Coulomb matrix elements which are small only at high magnetic fields ("adiabatic approximation"). It is well known that the valence-band structure in the plane of the well is quite anisotropic. We thus do not assume *a priori* that the quantum well is cylindrically symmetric ("axial approximation"), as is commonly done.[51–53,55–64] Within these ramifications we solve the exciton eigenvalue problem and discuss the reliability of the results. Our theory was first presented in Ref. 66 and several applications have already been published on different occasions.[22,25,67–70]

The paper is organized as follows. The theoretical framework is detailed in Sec. II, including a discussion of the symmetry of the problem and the computational method. In Sec. III the convergence properties of the basis set and the numerical accuracy of our calculations are discussed. Selected results are presented and discussed in Sec. IV, followed by the conclusions in Sec. V.

II. THEORETICAL FRAMEWORK

A. Effective-mass approximation

We are interested in the problem of Wannier excitons in quantum wells made from direct-gap cubic semiconductors in the effective-mass approximation.[71,72] We consider the situation of an s-type spin-degenerate state at the conduction-band edge and a sixfold degenerate state with p-type symmetry at the valence-band edge. The valence band is split by spin-orbit interaction into a fourfold degenerate ($J=\frac{3}{2}$) and a twofold degenerate ($J=\frac{1}{2}$) state, where J indicates the total angular momentum. The splitting is assumed to be so large that the interaction with the low-energy ($J=\frac{1}{2}$) state does not have to be calculated explicitly. Interactions between conduction and valence bands and couplings to more distant bands are also not explicitly included. An approximate treatment of the neglected nonparabolicities will be discussed in Sec. IV. If, additionally, the small departures from inversion symmetry are disregarded, the valence band is described by the so-called Luttinger Hamiltonian.[65] The band edges of the well are assumed to lie within the band gap of the barrier (type-I quantum well). The quantum-well potential is approximated by a square well at the interfaces. For the conduction band the boundary conditions at the interface are well described by the requirement of current continuity.[73] Although the boundary conditions for the valence band are less well established, we will employ those proposed in Refs. 74–76 which give results which agree well with those from tight-binding models.[76] We restrict attention to the situation where stress and electric and magnetic fields are oriented parallel to the quantum-well growth direction. Calculations will be carried out for (Ga,Al)As quantum wells only, but the theory is applicable to several other III-V systems as well.

In the effective-mass approximation[71,72] the μth eigenstate of an exciton at rest in a quantum well can be written as

$$\Psi^{\mu}_{\rm ex}(\mathbf{r}_e,\mathbf{r}_h)=\frac{\Omega}{\sqrt{A}}\sum_{M,M'}F^{\mu}_{M,M'}(\boldsymbol{\rho},z_e,z_h)\psi^{c}_{M}(\mathbf{r}_e)\hat{K}\psi^{v}_{M'}(\mathbf{r}_h)\ , \tag{1}$$

where Ω is the total volume of the system and A the area of the quantum well. The arguments in Eq. (1) are the coordinates of electron and hole $\mathbf{r}_e=(x_e,y_e,z_e)$ and $\mathbf{r}_h=(x_h,y_h,z_h)$ and the difference coordinates in the plane of the well $\boldsymbol{\rho}=(x_e,y_e,0)-(x_h,y_h,0)$. $\psi^{c}_{M},\psi^{v}_{M'}$ denote the Bloch functions of conduction- and valence-band electrons at the direct band gap, where M and M' are magnetic quantum numbers, i.e., $M=(-\frac{1}{2},\frac{1}{2})$ for the conduction band and $M'=(-\frac{3}{2},-\frac{1}{2},\frac{1}{2},\frac{3}{2})$ for the valence band. $\hat{K}$ denotes the time inversion operator which transforms the Bloch function of the valence-band electron into that of a hole. $F^{\mu}_{MM'}$ are the components of the μth exciton envelope function which diagonalizes the effective-mass-type Hamiltonian $\mathcal{H}_{\rm ex}$:

$$\sum_{L,L'}(\mathcal{H}_{\rm ex})_{MM',LL'}F^{\mu}_{LL'}=E^{\mu}_{\rm ex}F^{\mu}_{MM'}\ . \tag{2}$$

We shall neglect the electron-hole exchange interaction which is very small in GaAs (<0.1 meV). The eight-dimensional matrix equation (2) then reduces to two four-dimensional equations for spin-up and spin-down conduction-band electrons, respectively. $\mathcal{H}_{\rm ex}$ consists of

the effective-mass kinetic and magnetic energies of conduction-band electron and valence-band hole, the screened Coulomb interaction between electron and hole, square-well potentials for conduction and valence bands, and the potentials due to strains and electric fields.

The oscillator strength for an optical transition involving an exciton state described by Eq. (1) is given by[72]

$$f_{\rm ex}^{\mu}=\frac{2}{m_0}\frac{A}{E_{\rm ex}^{\mu}+E_g}\times\left|\sum_{M,M'}\langle\psi_M^c\,|\,\xi\cdot\pi\,|\,\psi_{M'}^v\rangle\int dz\,F_{MM'}^{\mu}(0,z,z)\right|^2, \tag{3}$$

where A denotes the area of the quantum-well interface, E_g the band gap of the bulk crystal of the well material, ξ the photon polarization, π the electron momentum operator, and m_0 the bare electron mass.

B. Symmetry

Before discussing the detailed structure of the exciton Hamiltonian we will have a look at its symmetry[77,78] which is useful for the classification of eigenstates as well as a means of reducing the computational effort when solving the eigenvalue problem. The latter aspect will be discussed at the end of Sec. II C. Complications due to the exchange interaction[78] will not be treated here.

In Table I the symmetry point groups of a [001] quantum well are compiled. The group of the effective-mass Luttinger Hamiltonian is equal to that of the diamond crystal for the bulk, ignoring the microscopic lack of inversion symmetry in GaAs which causes only small effects. The approximation of the quantum well by a square-well potential also leads to a symmetry which is higher than that of a quantum-well crystal, where the S_4 symmetry element is broken microscopically at the interfaces. Unlike a uniaxial stress in the same direction this in principle leads to, e.g., a very small mixing of heavy and light holes even at the center of the Brillouin zone as evidenced by, e.g., tight-binding calculations.[79] The symmetry is broken on a length scale of the order of the lattice constant which may be safely neglected in an effective-mass theory, however. Applied electric fields can significantly modify the potentials on the length scale of the envelope functions and the corresponding reduction of the symmetry must be taken into account. If directed along the crystal growth direction magnetic fields and applied stresses do not modify the spatial symmetry of the quantum well. A magnetic field then only splits the twofold (Kramer) degenerate exciton states. The point groups of the effective-mass Hamiltonian for [110] and [111] quantum wells are D_{2h} and D_{3d}. The microscopic crystal symmetry is also lower in these cases.

TABLE I. Symmetry point groups of [001] quantum wells.

	Microscopic	Luttinger
Bulk crystal	T_d	O_h
Quantum well	D_{2d}	D_{4h}
Quantum well + [001] Electric field	C_{2v}	C_{4v}
Quantum well + [100] Stress	C_2	D_{2h}

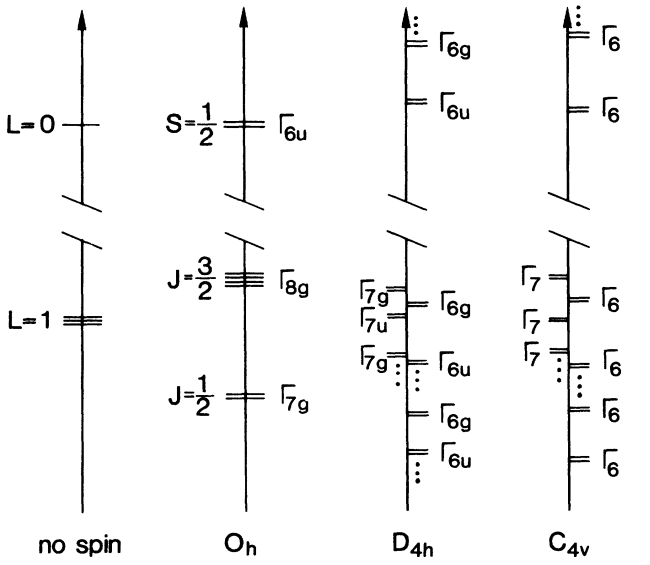

FIG. 1. Splitting of the band edges of a tetrahedral semiconductor by a quantum-well potential and an electric field in the [001] direction (cf. Table I).

In Fig. 1 degeneracies and energy-level splittings of the states at the band edges are depicted for a [001] quantum well, using the irreducible representation labels of the relevant double groups. The states labeled Γ_6 and Γ_7 are the light- and heavy-hole subband states at the zone center. In the presence of inversion symmetry the indices are augmented by g or u to indicate the parity of the state in question. Exciton states described by Eq. (1) transform according to the direct product of electron and hole Bloch functions and the exciton envelope function. Excitons are in the following labeled by the direct product of hole Bloch and exciton envelope function, which is possible because we neglect the electron-hole exchange interaction. By this convention (which is slightly different from that used in Ref. 68) exciton states also transform like Γ_6 and Γ_7, though they cannot unambiguously be classified as light or heavy anymore.

Exciton selection rules can be derived easily by the requirement that the direct product of exciton and photon representation contains the identity. Using the convention explained above only *gerade* states can have oscillator strengths in one-photon processes when the system possesses inversion symmetry. Γ_7-type excitons can be created only by light polarized in the plane of the well (σ polarization), while Γ_6-type excitons are observable also for polarization parallel to the growth axis (π polarization).

C. Matrix representation of exciton Hamiltonian

The exciton Hamiltonian is readily written down for quantum wells grown in the [001], [110], and [111] direc-

tions using the results of Ref. 77. Energies, measured relative to the band gap of the bulk material, will be expressed in units of rydbergs (R_0), lengths in hydrogen Bohr radii (a_0), and magnetic fields in terms of the dimensionless quantity γ:

$$R_0=\frac{m_0e^4}{2\hbar^2},\quad a_0=\frac{\hbar^2}{m_0e^2},\quad \gamma=\frac{e\hbar H}{2m_0cR_0}\ , \tag{4}$$

where all symbols have the usual meaning. For a [001] quantum well the exciton Hamiltonian reads

$$\mathcal{H}_{\rm ex}=\begin{bmatrix} A_{-3/2} & B & C & 0\\ B^* & A_{-1/2} & 0 & C\\ C^* & 0 & A_{1/2} & -B\\ 0 & C^* & -B^* & A_{3/2}\end{bmatrix} + \left[-\frac{2}{\epsilon\,|\mathbf{r}_e-\mathbf{r}_h|}\pm\frac{g_e}{2}\gamma\right]\underline{I}_4\ , \tag{5}$$

where

$$A_{\pm3/2}=-\frac{m_0}{m_e}\frac{\partial^2}{\partial z_e^2}+V_c(z_e)-(\gamma_1-2\gamma_2)\frac{\partial^2}{\partial z_h^2}+V_v(z_h)-(z_e-z_h)\Phi+\tfrac{2}{3}(S_{11}-S_{12})D_uT + \left[\gamma_1+\gamma_2+\frac{m_0}{m_e}\right]\left[-\nabla_\rho^2+\frac{\gamma^2\rho^2}{4}\right]+\left[-\gamma_1-\gamma_2+\frac{m_0}{m_e}\right]\gamma L_z\pm(3\kappa+\tfrac{27}{4}q)\gamma\ , \tag{6}$$

$$A_{\pm1/2}=-\frac{m_0}{m_e}\frac{\partial^2}{\partial z_e^2}+V_c(z_e)-(\gamma_1+2\gamma_2)\frac{\partial^2}{\partial z_h^2}+V_v(z_h)-(z_e-z_h)\Phi-\tfrac{2}{3}(S_{11}-S_{12})D_uT + \left[\gamma_1-\gamma_2+\frac{m_0}{m_e}\right]\left[-\nabla_\rho^2+\frac{\gamma^2\rho^2}{4}\right]+\left[-\gamma_1+\gamma_2+\frac{m_0}{m_e}\right]\gamma L_z\pm(\kappa+\tfrac{1}{4}q)\gamma\ , \tag{7}$$

$$B=-2i\sqrt{6}\gamma_3k^-\frac{\partial}{\partial z_h}\ , \tag{8}$$

$$C=\sqrt{3}(\gamma_2+\gamma_3)(k^-)^2+\sqrt{3}(\gamma_2-\gamma_3)(k^+)^2\ . \tag{9}$$

Here γ_1, γ_2, γ_3, κ, and q are the Luttinger[65] valence-band parameters, m_e and g_e are the effective-mass and g factor of the conduction-band electron, and $\underline{I}_4$ denotes the 4×4 unit matrix. If the difference coordinates of electron and hole $\mathbf{r}=\mathbf{r}_e-\mathbf{r}_h$ are expressed in cylindrical coordinates $(\rho,z_e-z_h)=(\rho,\phi,z_e-z_h)$ the raising and lowering operators k^+ and k^- introduced above read

$$k^\pm=\frac{i}{\sqrt{2}}e^{\pm i\phi}\left[\frac{\partial}{\partial\rho}\pm\frac{i\partial}{\rho\partial\phi}\pm\frac{\gamma\rho}{2}\right]\ . \tag{10}$$

L_z is the operator for the orbital angular momentum in the z direction

$$L_z=\frac{\partial}{i\partial\phi} \tag{11}$$

and ∇_ρ^2 is the two-dimensional Laplacian in the plane of the quantum well

$$\nabla_\rho^2=\frac{\partial^2}{\partial\rho^2}+\frac{1}{\rho}\frac{\partial}{\partial\rho}+\frac{1}{\rho^2}\frac{\partial^2}{\partial\phi^2}\ . \tag{12}$$

Neglecting effects due to the small difference in the dielectric constants of well and barrier materials, the electron-hole Coulomb interaction is assumed to be screened by the static dielectric constant ϵ. Φ denotes a constant electric field normal to the interfaces. The elastic compliance constants S_{11} and S_{12} and the deformation potential D_u parametrize the energy splittings of light- and heavy-hole bands at the zone center as a function of a uniaxial stress T normal to the well.

To ensure hermiticity, the operators which contain derivatives should be interpreted as[76]

$$A(z)\frac{\partial^2}{\partial z^2}\to\frac{\partial}{\partial z}A(z)\frac{\partial}{\partial z}\ ,$$
$$B(z)\frac{\partial}{\partial z}\to\frac{1}{2}\left[B(z)\frac{\partial}{\partial z}+\frac{\partial}{\partial z}B(z)\right] \tag{13}$$

at the interfaces.

D. Expansion of the exciton envelope function

The eigenvalue problem can be solved by expanding the exciton envelope function into a sufficiently large basis and diagonalizing the corresponding Hamiltonian matrix. The envelope functions in Eq. (2) can be expanded as follows:

$$F^\mu_{MM'}(\boldsymbol{\rho},z_e,z_h)=\sum_{n,m,i,j}c^{\mu MM'}_{nmij}\zeta_i^M(z_e)\zeta_j^{M'}(z_h)R_{nm}(\boldsymbol{\rho})\ . \tag{14}$$

$\{R_{nm}\}$ is a set of basis functions in the (ρ,ϕ) plane and the ζ's denote the subband envelope functions of the quantum well in the absence of electric fields. For the conduction band we have

$$\left[-\frac{m_0}{m_e}\frac{\partial^2}{\partial z_e^2}+V_c(z_e)\right]\zeta_i^M(z_e)=\varepsilon_i^M\zeta_i^M(z_e)\ , \tag{15}$$

while the $\zeta_j^{M'}(z_h)$ are the heavy- and light-hole subband envelope functions:

$$\left[-\frac{m_0}{m_h^{M'}}\frac{\partial^2}{\partial z_h^2}+V_v(z_h)\right]\zeta_j^{M'}(z_h)=\varepsilon_j^{M'}\zeta_j^{M'}(z_h)\ . \quad (16)$$

For a [001] quantum well $m_0/m_h^{\pm 3/2}=(\gamma_1-2\gamma_2)$ and $m_0/m_h^{\pm 1/2}=(\gamma_1+2\gamma_2)$. A realistic quantum well does not support more than a few bound states which in general do not provide sufficient variational flexibility in the expansion Eq. (14), and continuum states are computationally inconvenient. We therefore introduce infinite potential wells at both sides of the quantum well which are sufficiently far away to not disturb the bound subband states. Assuming current continuity at the (inner) interfaces Eqs. (15) and (16) are easily solved analytically for this double square-well system with a convenient discrete eigenvalue spectrum.

We propose to use the eigenfunctions of a two-dimensional system as the basis for the radial functions in the plane of the well. The bound-state wave functions of a two-dimensional hydrogen atom read[30]

$$R_{n,m}(\rho)=\frac{2}{a}\left[\frac{(n-|m|)!}{[(n+|m|)!]^3(2n+1)^3}\right]^{1/2}\times e^{-(r/a)/(2n+1)}\left[\frac{2\rho}{(2n+1)a}\right]^{|m|}\times L_{n-|m|}^{(2|m|)}(2\rho/[(2n+1)a])\frac{e^{im\phi}}{\sqrt{2\pi}}\ , \quad (17)$$

where $L_n^{(\alpha)}$ denotes an associated Laguerre polynomial and a is a length parameter. An expansion of the quantum-well excitons in terms of the orthogonal functions defined by Eq. (17) does not work well because the bound states of the Coulomb potential do not form a complete set. But the unbound (scattering) excitonic states can be dealt with variationally by a (nonorthogonal) expansion into bound states with different length parameters a. For zero and intermediate magnetic fields this basis performs satisfactorily, as borne out by the tests to be described in Sec. III B. It should be kept in mind that rapid convergence can be expected only when magnetic fields are not too strong ($H \lesssim 10$ T), i.e., as long as the magnetic length $(\hbar c/eH)^{1/2}$ is not much smaller than the exciton radius in the plane of the well.

It is difficult to cope with excitons which are associated with a higher subband edge and which interact with an exciton continuum associated with a lower subband edge (Fano resonance) without introducing additional approximations. In the present variational approach the continuum is replaced by a rather small number of discrete states. The energy position of a resonance can be traced easily, but the small energy shifts and broadenings discussed in Ref. 52 are neglected. Note that the problematic continuum states vanish upon application of a magnetic field.

The next step is the calculation of the Hamiltonian matrix for the chosen basis. With the exception of the Coulomb interaction the matrix elements are readily obtained analytically. Using the method explained in Appendix I we have been able to reduce the Coulomb interaction matrix elements to a one-dimensional quadrature, which is essential for keeping the computations feasible. Since the basis is nonorthogonal, exciton wave functions and energies are obtained by solving a generalized eigenvalue problem.

Although straightforward in principle, an accurate numerical diagonalization of the Hamiltonian requires consideration of the symmetry of the problem. In Table II the basis functions are labeled according to their irreducible representations for a [001] quantum well. Trivially, in an expansion of a given exciton state only basis functions of one and the same symmetry have to be included, which means that (in the absence of an electric field) the dimension of the problem can be reduced by a factor of 4 by sole inspection of Table II. Next, it is helpful to neglect the cubic anisotropy in the (ρ,ϕ) plane, i.e., the $(k^+)^2$ operator in Eq. (5), for the moment. In that case the total angular momentum $\mathcal{M}$ in the z direction is a good quantum number (symmetry group $D_{\infty h}$). $\mathcal{M}$ is the sum of the angular momenta of the envelope function m and of the Bloch functions of electron M and hole $-M'$. Each envelope function component $F_{MM'}^{\mu}$ then has a definite angular momentum $m=\mathcal{M}-M+M'$. Thus s envelope ($m=0$) excitons from the $M'=\frac{3}{2}$ valence band only mix with p excitons ($m=-1$) from $M'=\frac{1}{2}$, d excitons ($m=-2$) from $M'=-\frac{1}{2}$, and f excitons ($m=-3$) from $M'=-\frac{3}{2}$. By the warping the axial symmetry is broken in favor of a fourfold symmetry axis which is easily seen to mix states with $m, m\pm 4, m\pm 8, \ldots$, but still the dimension of the eigenvalue problem is significantly reduced. Quantum wells grown on (111) or (110) surfaces contain a threefold and twofold symmetry axis, which means that warping induces mixings between $m, m\pm 3, m\pm 6, \ldots$ and $m, m\pm 2, m\pm 4, \ldots$, respectively. We thus see how the necessary computational effort increases with decreasing symmetry. External perturbations which break the crystal symmetry also render the calculations more difficult. The problem of, e.g., a uniaxial stress along [100] applied to a [001] quantum well, which mixes s-type excitons derived from the heavy- and light-hole bands,[24] is in the present effective-mass approximation formally equivalent to that of an unperturbed [110] quantum well.

Turning again to the oscillator strength, we can ex-

TABLE II. Representation labels of exciton basis in D_{4h}.

$\lvert m\rvert$	Parity $\zeta_e\zeta_h$	M'	Exciton label
$s,g,8,\ldots$	+	$\pm\frac{3}{2}$	Γ_{7g}
	+	$\pm\frac{1}{2}$	Γ_{6g}
	−	$\pm\frac{3}{2}$	Γ_{7u}
	−	$\pm\frac{1}{2}$	Γ_{6u}
$p,f,5,\ldots$	+	$\pm\frac{3}{2}$	Γ_{6u}
	+	$\pm\frac{1}{2}$	Γ_{7u}
	−	$\pm\frac{3}{2}$	Γ_{6g}
	−	$\pm\frac{1}{2}$	Γ_{7g}
$d,6,10,\ldots$	+	$\pm\frac{3}{2}$	Γ_{6g}
	+	$\pm\frac{1}{2}$	Γ_{7g}
	−	$\pm\frac{3}{2}$	Γ_{6u}
	−	$\pm\frac{1}{2}$	Γ_{7u}

press the integral over the envelope function in Eq. (3) in terms of the expansion in Eq. (14) as

$$\int dz F^{\mu}_{MM'}(0,z,z)=\sum_{n,i,j} c^{\mu MM'}_{n0ij} R_{n0}(0)\int dz \zeta^{M}_{i}(z)\zeta^{M'}_{j}(z)\ , \tag{18}$$

where use has been made of the fact that only the s-type ($m=0$) radial functions are nonzero at the origin. It follows from the above discussion that for [001] quantum wells the s component of the μth state can always be assigned to one of the four valence bands with index M'_{μ}:

$$f^{\mu}_{\rm ex}=f^{B}_{MM'_{\mu}}\frac{E_g}{E^{\mu}_{\rm ex}+E_g} \times A\left|\sum_{n,i,j} c^{\mu MM'_{\mu}}_{n0ij} R_{n0}(0)\int dz \zeta^{M}_{i}(z)\zeta^{M_{\mu'}}_{j}(z)\right|^2 , \tag{19}$$

where $f^{B}_{MM'}$ is the oscillator strength[80] of a band-to-band transition in the bulk crystal (see Fig. 2).

Finally it is necessary to fill in the empirical parameters of the theory. In Table III we list those used in the following calculations which consistently fit subband positions of differently oriented quantum wells.[81] This choice implies a band-offset rule which allocates 68% of the total band-gap difference to the conduction band. The band gap and effective masses of the (Ga,Al)As alloy are linearly interpolated as a function of the Al concentration between the values for GaAs and AlAs.

III. COMPUTATIONAL DETAILS

Even when full use is made of the symmetry as discussed above, a considerable computational effort is involved in solving the exciton eigenvalue problem accurately. In the following we will discuss the extent of the expansion which is necessary to obtain (numerically) reliable results and point out the limits of the present method. For the ground-state exciton energies a numerical accuracy of better than 0.1 meV can be achieved, at least for magnetic fields under 10 T. Illustrative results are presented for a GaAs/$Al_{0.3}Ga_{0.7}As$[001] quantum well with a width of 100 Å.

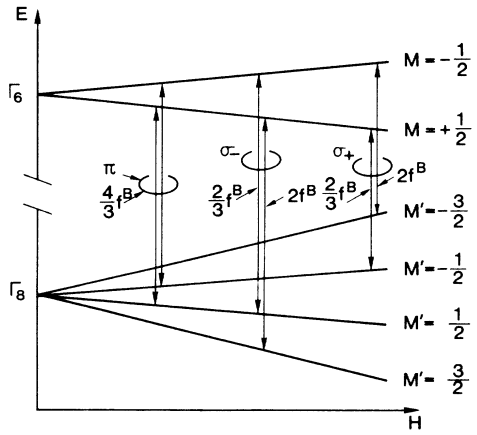

FIG. 2. Spin splittings and allowed interband transitions in bulk GaAs in a magnetic field ($g_e<0,\kappa>0$). f^B is the interband oscillator strength in Table III: $2\,|\langle\Psi^{c}_{1/2}|\pi_x|\Psi^{v}_{3/2}\rangle|^2/E_g m_0$.

TABLE III. Effective-mass parameters.

	GaAs	AlAs
m_e	0.0665	0.15
γ_1	6.790	3.790
γ_2	1.924	1.230
γ_3	2.681	1.395
E_g	1.519 eV	2.766 eV
κ	1.2	1.2
q	0.04	0.04
g_e	−0.44	−0.44
ϵ	12.5	12.5
$\frac{2}{3}(S_{11}-S_{12})D_u$	2.55 meV/kbar	2.55 meV/kbar
$f^{B}_{1/2,3/2}$ (unpol.)	9.48	9.48

A. Hole subbands

Figure 3 gives the subband dispersion of the holes in the plane of the well in the absence of any perturbations as calculated using the Luttinger Hamiltonian. The band structure is obtained simply by omitting the electron-hole attraction in Eq. (5) and by replacing the radial functions by plane waves in the basis. Using 30 subband envelope functions for light and heavy holes the results are virtually exact. The importance of the nondiagonal terms is obvious. The modification of the bands due to the warping is observed to be rather small.

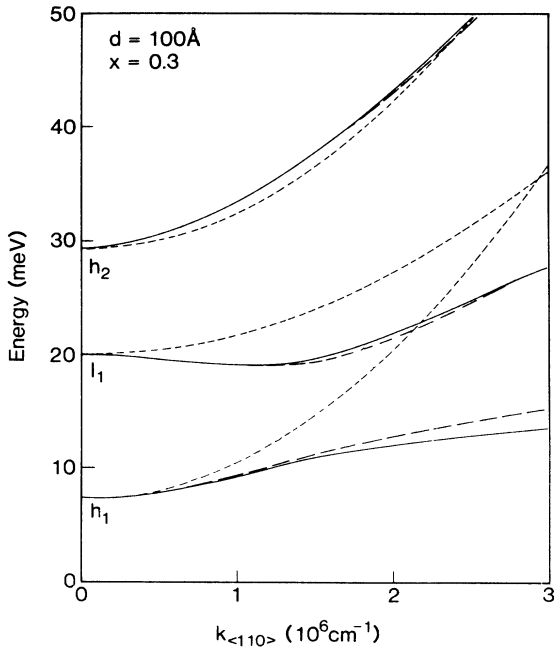

FIG. 3. Energy dispersion of valence-band holes in a quantum well as a function of the in-plane wave vector in the [110] direction. The solid curves give the results for the full Luttinger Hamiltonian while the dotted lines reflect the neglect of valence-band mixing. The dashed lines correspond to the neglect of the warping in the plane of the well.

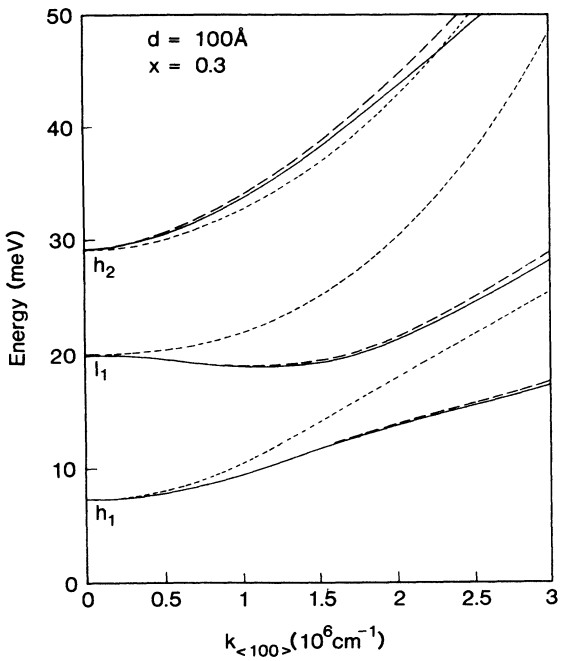

FIG. 4. Energy dispersion of valence-band holes in a quantum well as a function of the in-plane wave vector in the [100] direction. The solid curves give the results as obtained by diagonalizing the valence-band Luttinger Hamiltonian with a basis of 30 subbands envelope functions for heavy and light holes, while six bands have been employed to obtain the dashed lines. The dotted lines give the results for the minimal basis set of two heavy- and one light-hole subbands.

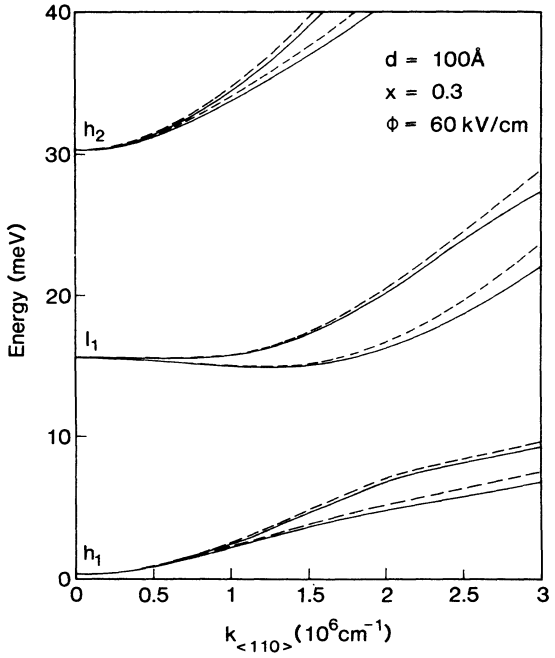

FIG. 5. Valence-band hole energy dispersion in a quantum well as a function of the in-plane wave vector in the [110] direction and in the presence of an electric field of 60 kV/cm normal to the well. Dashed and solid curves correspond to a basis set of 6 and 30 subbands, respectively.

The quality of the subband basis can be easily tested by calculations of the energy dispersion of the subbands in the plane of the well. From Fig. 4 it is clear that the subband envelope functions at the zone center are a rapidly converging basis set. In the exciton calculations we have to restrict the basis to about six bands for each hole type. We can deduce from Fig. 4 that this basis should be sufficient since excitons mainly sample band states with wave vectors up to about the reciprocal exciton radius ($\simeq 10^6$ cm^{-1}). The effects of electric fields on the subbands is shown in Fig. 5. When the potential drop over the quantum well is of the order of the barrier heights the quality of the basis is deteriorated, but in this limit the field ionization of the excitons is important and application of the present approach becomes questionable anyway.

B. Radial basis

As explained in Sec. II A we choose to expand the exciton envelope function in the plane of the well by hydrogenic wave functions. While this is the basis of choice for zero magnetic field problems, it is necessary to check its performance in the presence of magnetic fields. We shall work with two radial basis sets with length parameters listed in Table IV.

A severe test of the flexibility of the basis is a calculation of the Landau-level transitions, which are obtained when the Coulomb interaction between electrons and holes is switched off. In Fig. 6 we plot results for a model of parabolic hole bands using a heavy- and light-hole mass average. The results can be checked by comparison with the exact linear energy dispersion indicated by the dashed lines. Labels are chosen according to the quantum numbers (n,m) of the radial functions, where the angular momentum quantum numbers

$$m=(\ldots,-2,-1,0,1,2,\ldots)$$

are denoted as

$$m=(\ldots,d\text{-},p\text{-},s,p,d,\ldots)\ .$$

The label $(2p\text{-})$ for example corresponds to a transition between the second hole and first electron Landau level.[39] We observe that at 10 Tesla the basis set II is very accurate for main quantum numbers $n=1$ and 2, performs fairly well for $n=3$, only moderately for $n=4$, and fails

TABLE IV. Radial basis set exponents.

$(n, \lvert m \rvert)$	Set I (Å)	Set II (Å)
$1s,2s$	10 50 100 150 200	10 20 35 50 75 100 150 200
$2p,3d,4f$	2.5 12.5 25 37.5 50	2 8 14 20 26 32 38 44 50 60

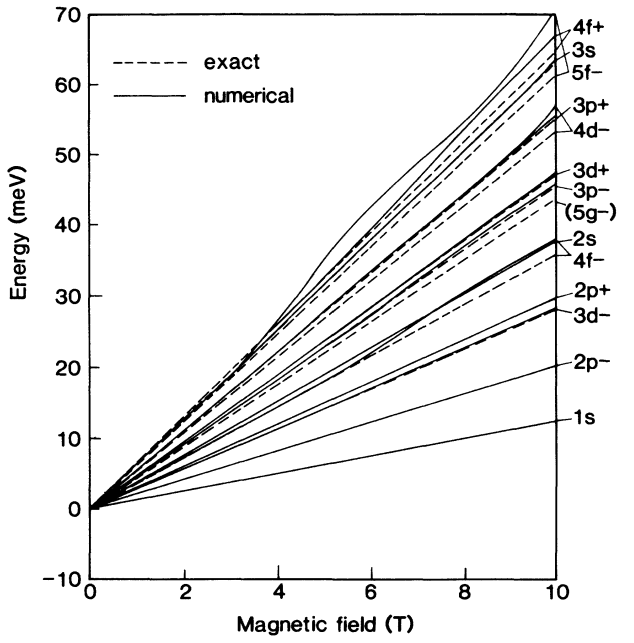

FIG. 6. Landau-level transition energies relative to the first subband energy gap in a quantum well as a function of a magnetic field. The parameters γ_2, γ_3, g_e, κ, and q are set equal to zero. The dashed lines give the exact results, while the solid curves are obtained with the present exciton program and basis set II (Table IV). The labels are the angular momentum quantum numbers (n,m) of the relative electron-hole motion, e.g., $2p\text{-}\!\rightarrow n=2, m=-1$.

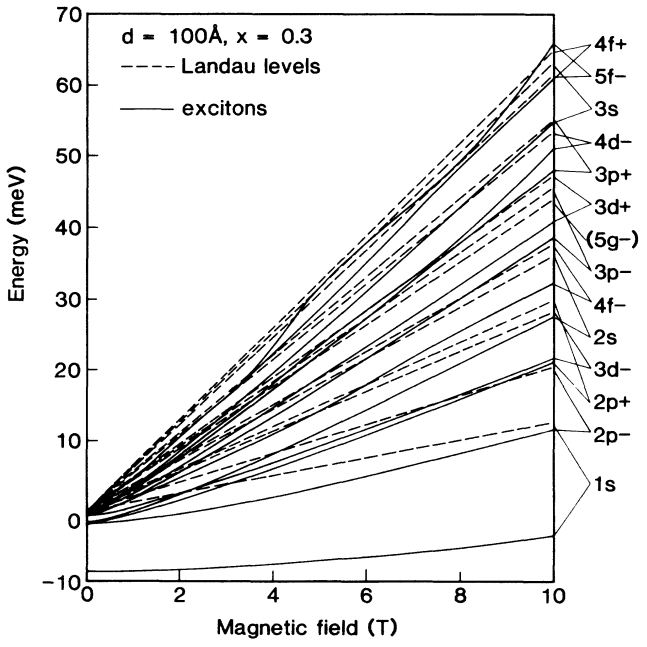

FIG. 7. Transition energies relative to the first subband edge in a quantum well as a function of a magnetic field (see Fig. 6). The solid curves are exciton transitions which are obtained by including the electron-hole Coulomb interaction. The coupling to higher subbands is neglected here.

for $n=5$. The reason for the discrepancies at higher energy is not so much the Gaussian falloff of the Landau-type wave function but its larger number of nodes. The performance of the smaller basis set I is satisfactory for zero-field problems. At 10 T a description as above can be used, provided that the quantum numbers n are reduced by one.

In Fig. 7 the calculations which led to Fig. 6 are repeated including the Coulomb interaction (but neglecting couplings to higher subbands). There are no analytical results to compare with now, but it is observed that even high Landau-level transitions are strongly modified by the electron-hole attraction. We thus expect that the convergence of our hydrogenic basis will be better for the excitons than for the Landau levels.

C. Excitons

The convergence properties of the expansion of the envelope function at a magnetic field of 10 T are summarized in Figs. 8 and 9 for the ground-state excitons associated with the four magnetic quantum numbers of the valence-band multiplet. The parameters g_e, κ, and q are set equal to zero in these calculations. The binding energies are defined relative to the zero-field subband energy. We monitor the effects of increasing the number of subbands for electron, heavy-hole and light-hole bands in the expansion of an envelope function component $F_{MM'}$, as well as the number of envelope function components, which, for fixed electron spin, is a number between 1 and 4.

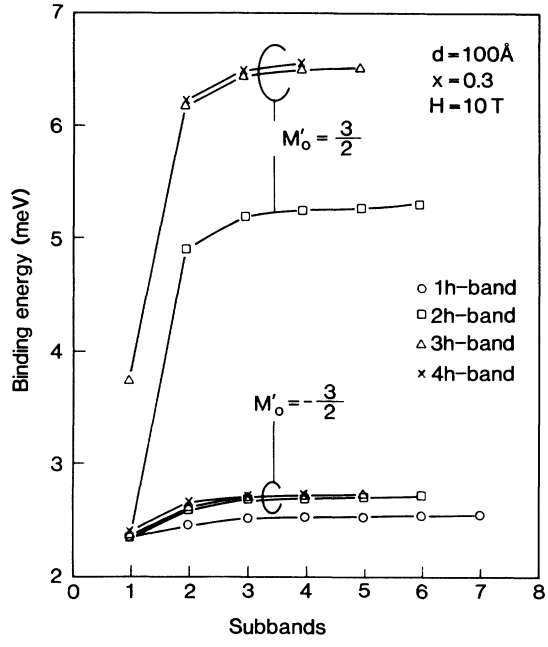

FIG. 8. Γ_{7g} (heavy-hole) exciton ground-state binding energies relative to the zero-field band edge at 10 T. The s-type envelope function component is associated with spin-up and spin-down heavy-hole valence bands ($M'_0=\pm\frac{3}{2}$). The ordinate is the number of subbands in the expansion of the exciton envelope functions. The different models are explained in the text.

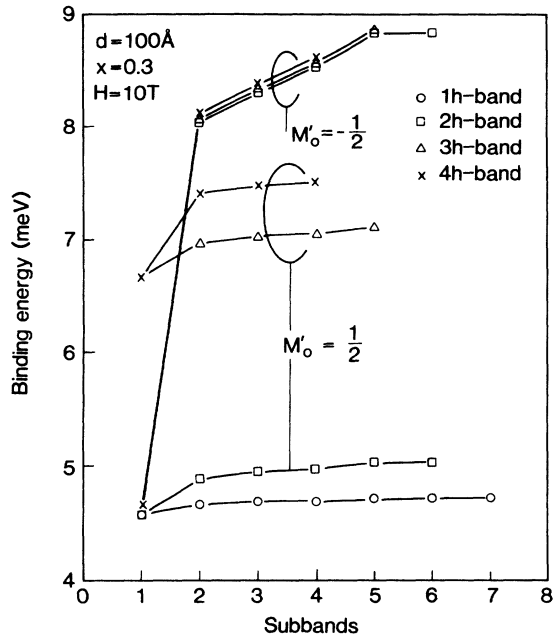

FIG. 9. As Fig. 8, but for Γ_{6g} (light-hole) excitons ($M_0'=\pm\frac{1}{2}$).

The calculations labeled $1h$ band refer to a model of one envelope function component only, which is equivalent to the neglect of all nondiagonal elements in the Luttinger Hamiltonian. Due to the neglect of κ and q the heavy- and light-hole excitons are spin degenerate in this case. By comparison with the full calculations we observe that this model is unsatisfactory. In the $2h$-band model the effect of the coupling of s- and p-type heavy- and light-hole excitons by the operator B in Eq. (5) is included. A strong spin splitting is induced which reflects the two different angular momenta of the p states to which the s-type excitons couple. In the $3h$-band model we also allow for interactions with excitons having d symmetry in the plane, but neglect the effect of warping. This is a good approximation for zero-field problems, but at 10 tesla the convergence is not complete. The results labeled $4h$ band include the coupling between all states in the multiplet up to f symmetry. The effect of warping is small in all cases ($\lesssim 0.05$ meV). We are, therefore, confident that the effects of warping for non-[001] quantum wells are also negligible. When the radial basis set I is used, a small but significant decrease (of the order of 0.1 meV) in the binding energies is observed. We may conclude from Figs. 8 and 9 that the $4h$-band model and a basis of about five subbands is in principle necessary to obtain well-converged results. Computational effort can be saved without introducing large errors by reducing the number of electron subbands. At zero magnetic field basis set I and the $3h$-band model usually suffices.

For a given basis set the convergence decreases with increasing magnetic field and depends only weakly on well width. For narrower wells our confidence in the subband expansion decreases because of the increased contribution of the continuum states, although Ekenberg and Altarelli[54] found the subband continuum admixture into the ground-state excitons to be negligible. The quality of the expansion decreases of course for higher excited states. We do not attempt to establish general rules here, but refer to Fig. 7 for the radial functions and note that for the second subband transition the number of subband expansion functions is effectively reduced by one.

IV. REPRESENTATIVE RESULTS AND DISCUSSION

In the following we present and discuss representative numerical results from the theory outlined in the preceding sections. We do not single out individual experiments here. The comparison with several experiments on quantum wells with different growth parameters has already been carried out successfully in Refs. 22, 25, and 66–70. In an attempt to give a comprehensive impression of the effects of exciton mixing we proceed as follows. The effects of the crystal-growth orientation are presented first as a function of well width. The effects of external perturbations on the other hand are illustrated for the "standard" 100 Å $GaAs/Al_{0.3}Ga_{0.7}As$[001] quantum well for which convergence properties have been discussed in Sec. III. From this it should be qualitatively clear what results are to be expected for different sample parameters and/or different combinations of external perturbations as pressure and magnetic fields.

To indicate the main character of an exciton (at the first electron subband) a notation as $h_j(n,m)$ and $l_j(n,m)$ is used, where j is the subband index of heavy (h) and light (l) holes and (n,m) are angular momentum quantum numbers, as before (see Sec. III B). In all cases the same state of the art parameter set[81] in Table III and 68/32 band offsets have been employed (which do not necessarily give best agreement with all experiments, however[69]). In all cases the width of the infinite potential well which eliminates the subband continuum exceeds the quantum-well width by 250 Å.

A. Crystal growth direction and well width dependence

The results of our calculations for heavy- and light-hole excitons are presented in Figs. 10–14 as a function of quantum-well crystal orientation and well width ($3h$-band model, four electron plus six holes subband basis, radial basis I, cf. Sec. III C). Also displayed are the results as obtained in the two-band model where valence-band mixing is neglected (though Coulombic couplings between excitons at different subbands are included). Ground-state energies of Γ_{7g} (predominantly heavy-hole) excitons and their oscillator strengths for unpolarized light with wave vectors normal to the well are plotted in Figs. 10 and 11. The oscillator strengths for [001] quantum wells differ by a scale factor from our previously published ones,[66] which had been obtained for a different f^B and light polarization. In Fig. 12 binding energies of Γ_{7g} first excited ($2s$) excitons are given. The effects of mixings, crystal direction, and well width are small, which lends credit to the method of measuring exciton

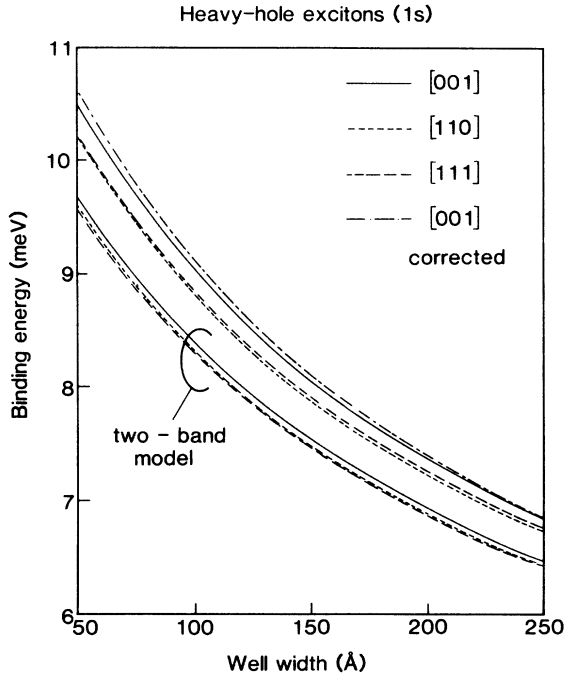

FIG. 10. Γ_{7g} (heavy-hole) ground-state exciton binding energies of $GaAs/Al_{0.3}Ga_{0.7}As$ quantum wells grown along the main crystal directions. The two-band model corresponds to the neglect of exciton mixing. The dot-dashed line is corrected for electron nonparabolicity.

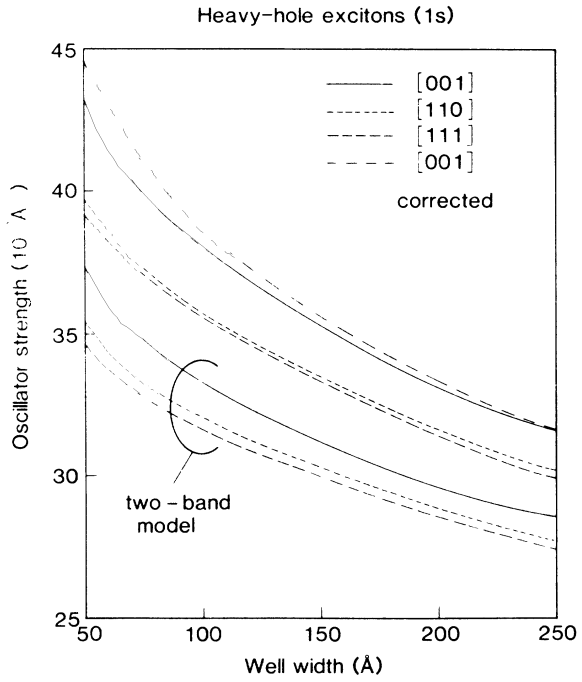

FIG. 11. Oscillator strengths of the exciton transitions in Fig. 10 for unpolarized light incident normal to the well.

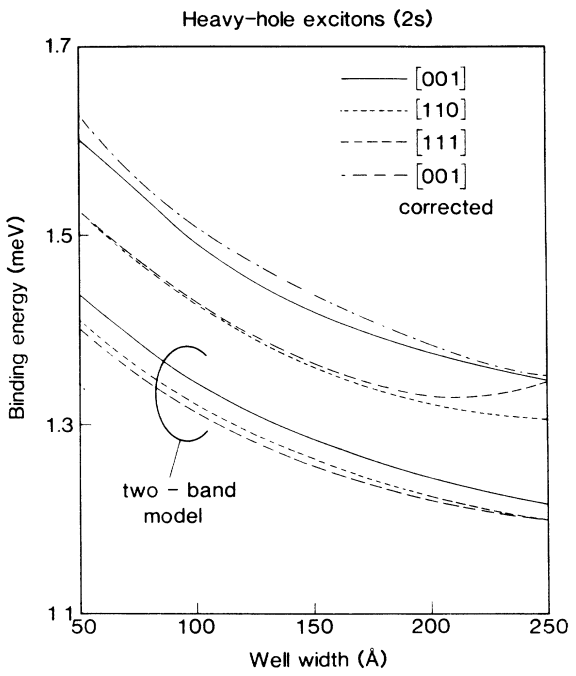

FIG. 12. As Fig. 10, but for the first ($2s$) excited state of Γ_{7g} (heavy-hole) excitons.

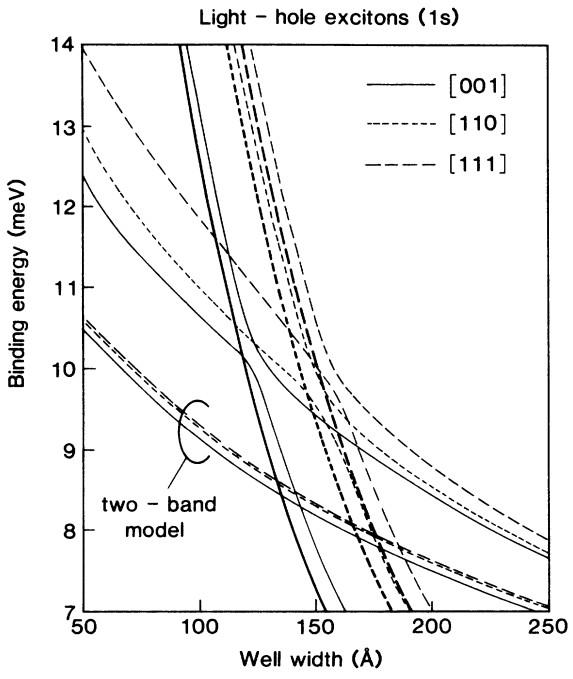

FIG. 13. Binding energies of Γ_{6g} (light-hole) excitons relative to the light-hole band edges of $GaAs/Al_{0.3}Ga_{0.7}As$ quantum wells grown along the main crystal directions. Solid lines indicate the position of the first heavy-hole subband edges. Anticrossing with $h_1(3d)$ is displayed but mixing with other d states is omitted. The two-band model corresponds to the neglect of exciton mixing.

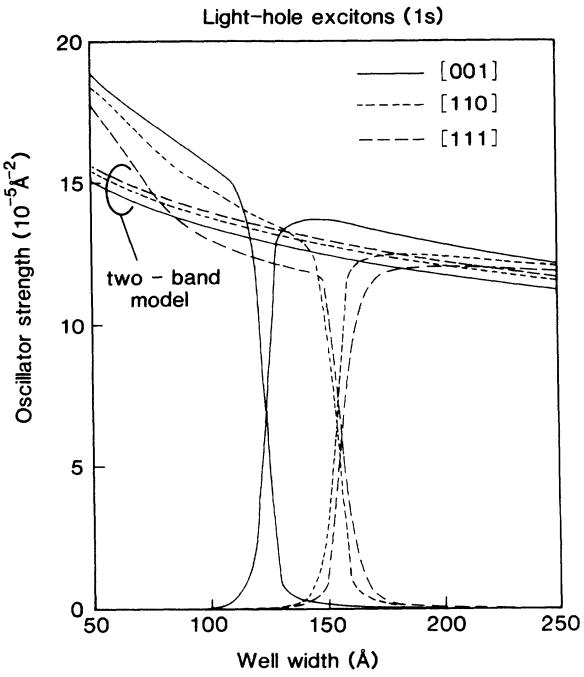

FIG. 14. Oscillator strengths of the exciton transitions in Fig. 13 for an unpolarized light incident normal to the well.

binding energies via $1s$-$2s$ term splittings.[6,7,28] Note the sudden increase of the binding energy at large well widths for the [111] system which is caused by interactions with excitons associated with the third heavy-hole subband. Although this effect is hardly observable, it indicates that interesting mixing effects can be expected for still larger well widths, but we are not aware of experimental work in this direction. The binding energy of $h_1(3s)$ is calculated to vary between 0.52 and 0.61 meV for the investigated well widths and crystal orientations.

The effect of the electron nonparabolicity has been estimated by employing the electron effective masses at the bottom of the first subband as calculated by the eight-band $\mathbf{k}\cdot\mathbf{p}$ method from Refs. 75 and 76. The effects on the binding energy are quite different from the results of previous work, being smaller and less dependent on well width. This is probably due to the consistent treatment of the nonparabolicities in well and barrier materials, which partly cancel and compensate well width dependences. Following suggestions in Ref. 76 we have also tried to incorporate the effect of the light-hole nonparabolicity by using subband-energy-dependent Luttinger parameters. It turned out that such an approach is meaningful only in the limit of a very large spin-orbit splitting, which is not realistic for the present system. The effect on the exciton binding energies is probably significant in the neighborhood of exciton anticrossings only.

The results for the $l_1(1s)$ binding energies are given in Fig. 13. The position of the first heavy-hole subband continuum is indicated by heavy lines. The light-hole s-type exciton mixes with the heavy-hole d-type excitons, which leads to the anticrossing close to the band edge.[66] This is more evident in the oscillator strengths (Fig. 14). If separated in energy from $l_1(1s)$ the oscillator strength of the $h_1(3d)$ is very weak, but close to crossing the light-hole exciton line will split into a doublet. This borrowing of oscillator strength of $h_1(3d)$ from $l_1(1s)$ has recently been observed.[22] When the light-hole exciton merges with the continuum a Fano resonance occurs. The lines in Fig. 13 inside the heavy-hole continuum trace the approximate location of the resonance as obtained from a numerical "dediagonalization" of the s-type light-hole exciton and the unbound heavy-hole states with d character. The higher excited but bounded $h_1(4d)$, etc. states are so closely spaced in energy that we treat them like the continuum.

It is well known by now that valence-band couplings are more important for the light-hole than for the heavy-hole bands, causing electronlike effective masses at the zone center (Fig. 3). In agreement with previous theories we find indeed a larger binding energy, with more significant effects of exciton mixing. There is also a clear dependence on the quantum-well crystal orientation, which is easily understood as follows:[24] The $h_2(2p)$ exciton turns out to strongly mix with the ground state of the light-hole exciton $l_1(1s)$. The anisotropy of the light-hole exciton binding energy can thus be traced to the strong anisotropy of the second heavy-hole subband energy. In the [111] direction the second heavy-hole subband energy is minimal and pushes the light-hole exciton to lower energies, causing a larger binding energy. The oscillator strength of the exciton in [111] quantum wells (Fig. 14) is smaller than that of the other directions, which is caused by the increased $h_2(p)$ component, which has no oscillator strength in itself.

The effect of mixing on the exciton ground states is not very dramatic, so that perturbation theory can be applied, and limitations of the basis also do not seriously affect the results. The present binding energies for the [001] direction are therefore only a few tenths of an meV larger than those of comparable theories.[53–55] But there is mounting evidence[6,7,22,25] that theory underestimates ground-state exciton binding energies by $\simeq 1-1.5$ meV. Duggan[6,40] obtains good agreement with experiment using a two-band model of impenetrable potential barriers and a heavy-hole parallel mass of 0.18, but his approximations are known to overestimate binding energies. It has been claimed[82] that polaron corrections to exciton binding energies can explain the discrepancies. But polaron corrections to the exciton binding are completely negligible for the bulk. The enhancement of polaron corrections in the quantum well is according to our estimates clearly too small to achieve agreement between theory and experiment. Corrections due to image potentials are also estimated to be very small considering the small difference in dielectric constant between GaAs and (Al,Ga)As alloy and the rather wide wells considered here. It is thus tempting to ascribe the discrepancies to the neglect of "central-cell corrections," which are quite significant in the case of shallow impurities with comparable binding energies.

B. Pressure and electric field effects

Stress applied in the growth direction of a [001] quantum well shifts the heavy-hole subband relative to the

light-hole subband.[58] The subband order can be reversed with a relatively small external pressure of a few kbar. In the present context pressure effects are interesting because of the anticrossings expected due to the exciton mixing. Note that mixings observed in Refs. 18 and 24 are not treated here because they originate from pressure applied parallel to [001] quantum wells which breaks the fourfold rotational symmetry.

In Fig. 15 the main exciton peaks with nonzero oscillator strengths and subband edges of heavy- and light-hole excitons are plotted as a function of the external stress for our standard quantum well (basis as in Sec. IV A). As in Fig. 13, anticrossings are calculated between $h_1(3d)$ and $l_1(1s)$, $l_1(2s)$ as well as between $l_1(3d)$ and $h_1(1s)$, $h_1(2s)$. Parity-forbidden exciton states like $l_1(2p)$ and $h_1(2p)$ gain oscillator strength when an electric field is switched on. Also, new anticrossings can be expected[67,68] when the subband edges are tuned through each other as indicated in Fig. 16. The mixings involving $3p$ states (not shown) are very weak. Utilizing the external pressure effects, field-induced anticrossings reported by Viña *et al.*[19] should be observable also for other sample parameters. Note the anomalous behavior of $l_1(2p)$ caused by the interaction with $h_2(1s)$, which decreases with increasing pressure.

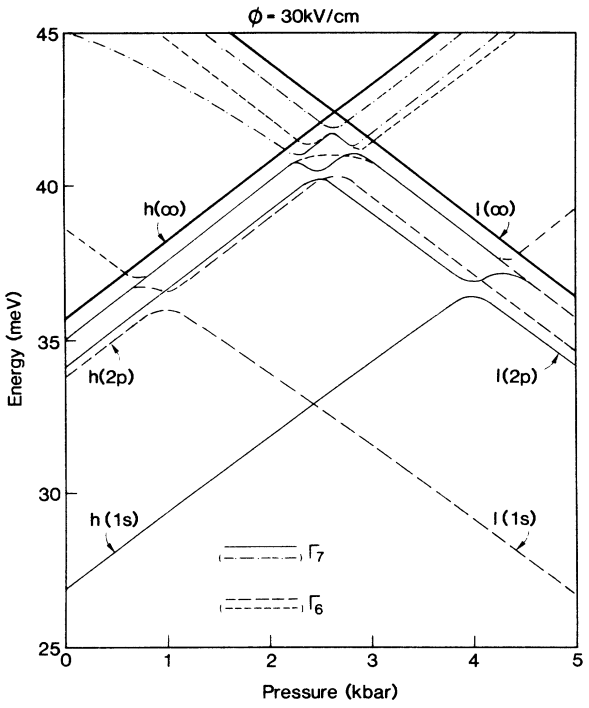

FIG. 16. As Fig. 15, but in the presence of an applied electric field of 30 kV/cm.

C. Magnetic field effects

The main effects of a magnetic field are a parabolic confining potential in the plane of the well and a splitting of the (Kramers) spin degeneracy of the exciton states. The magnetic confinement leads to an enhancement of the oscillator strengths, especially of weakly bound excited exciton states, and a large number of them may become observable. The energy shifts of the different excitons are also very different, resulting in complicated patterns in the spectral fans. Results for our standard quantum well are depicted as a function of magnetic field in Figs. 17–21. They have been obtained with a basis of six subband states for the holes and the radial basis II. To save computer space and time only two electron subbands are included which causes for the present well width errors of about 0.05 meV. Warping is neglected, but all other couplings up to f symmetry are included. Exciton states are plotted separately according to their group representation labels Γ_{7g}, Γ_{6g}, Γ_{7u}, and Γ_{6u} and the spin direction of the hole. The full lines correspond to the hole "spin-up" states, i.e., the s component belongs to the valence band with $M'=-\frac{3}{2}$ or $M'=-\frac{1}{2}$, while the dashed lines denote the "spin-down" states $M'=\frac{3}{2},\frac{1}{2}$. The spin directions can be observed separately by polarization analysis of the light in the Faraday configuration, as indicated in Fig. 2. The electron g factor is too small to cause observable effects on the energy scale in Figs. 17–20 ($\simeq 0.1$ meV).[69] The *ungerade* exciton transitions are strictly forbidden in one-photon experiments on symmetric quantum wells, but they are the observable ones in two-photon spectroscopy.[26,50] There are also indications[69] that mechanisms exist which render forbidden transitions visible, like unintentional imperfections or residual electric fields. Also it is possible to transfer oscillator strength from allowed to forbidden transitions by an intentional application of an electric field, as discussed above. The states with large radial quantum numbers which are not calculated accurately because of basis set

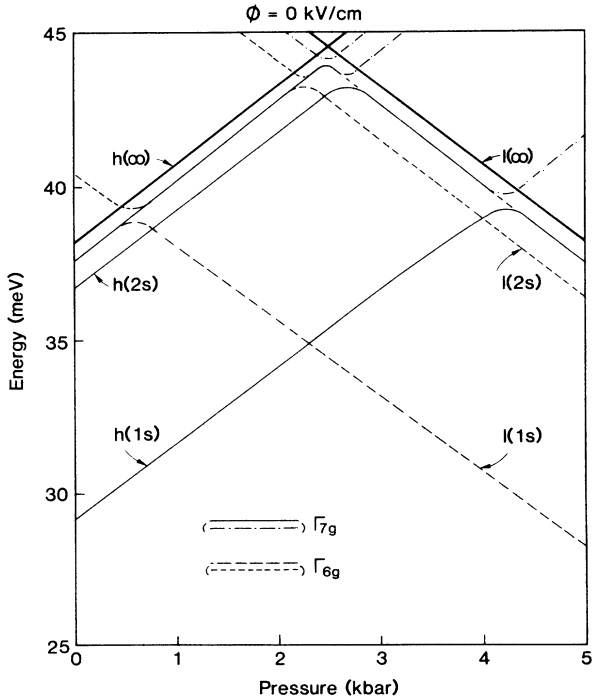

FIG. 15. Exciton energies as a function of uniaxial pressure of a 100 Å [001] $GaAs/Al_{0.3}Ga_{0.7}As$ quantum well. $h(\infty)$ and $l(\infty)$ denote the subband edges of heavy- and light-hole transitions.

limitations (see Sec. III B) are to a large extent removed from the figures. We do not expect qualitatively new results from a further increase of the basis set and accept here a numerical error in the energies of the plotted higher excited states which is estimated to amount to up to a few meV.

The character of different exciton states in Figs. 17–20 is given at zero magnetic field. Except at obvious anticrossings it is often possible to identify exciton character up to quite high magnetic fields. The spin splittings of the exciton ground states are similar to that of wider wells[69,70] although the crossing of Γ_{7g} ground states as found by Ossau *et al.*[14,61] occurs at much higher fields for the present parameter set. The spin splittings are incompatible with the bulk g factors of electron and holes which can be satisfactorily explained as a mixing effect with excited exciton states.[69,70] The assumption of modified Luttinger parameters[27] is thus not necessary. The splittings of $h_1(2s)$ and $h_3(1s)$ are again[69] of opposite sign compared to $h_1(1s)$. In Fig. 21 the oscillator strengths of the Γ_{7g} ground states and, at fields over 1 T, the ground and first excited states of Γ_{6g} are plotted. At low magnetic fields the oscillator strength of the Γ_{6g} excited state in Fig. 21 represents an integral over the $l_1(1s)$ resonance in the heavy-hole quasi-continuum. The Γ_{7g} ground state consists predominantly of $h_1(1s)$. The spin-down ($M'=\frac{3}{2}$) oscillator strength is slightly smaller than that of the spin-up exciton because of the relative vicinity of $h_1(3d$-) and $l_2(2p$-). The ground state of Γ_{6g} starts as predominantly $h_1(3d)$, and changes into $l_1(1s)$ with increasing field. In contrast to Yang and Sham[61] we find

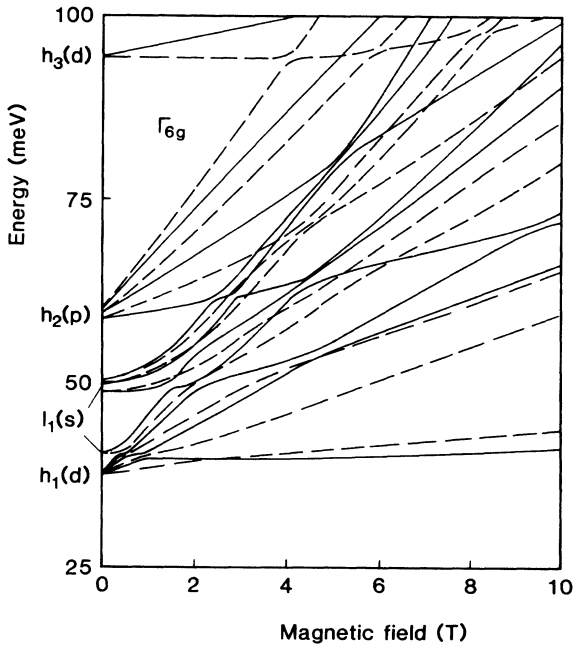

FIG. 18. Γ_{6g} exciton energies of a 100 Å, [001] $GaAs/Al_{0.3}Ga_{0.7}As$ quantum well as a function of magnetic field. The solid (dashed) lines denote association of the s-type envelope function components with $M'=-\frac{1}{2}$ ($M'=\frac{1}{2}$).

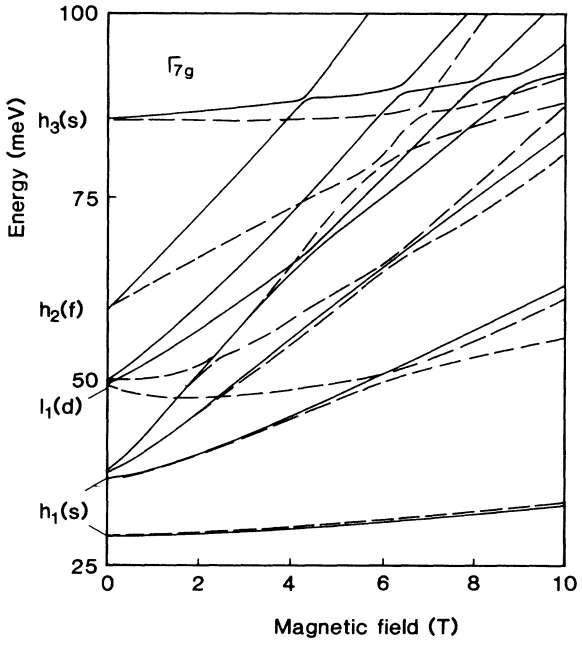

FIG. 17. Γ_{7g} exciton energies of a 100 Å, [001] $GaAs/Al_{0.3}Ga_{0.7}As$ quantum well as a function of magnetic field. The solid (dashed) lines denote association of the s-type envelope function components with $M'=-\frac{3}{2}$ ($M'=\frac{3}{2}$).

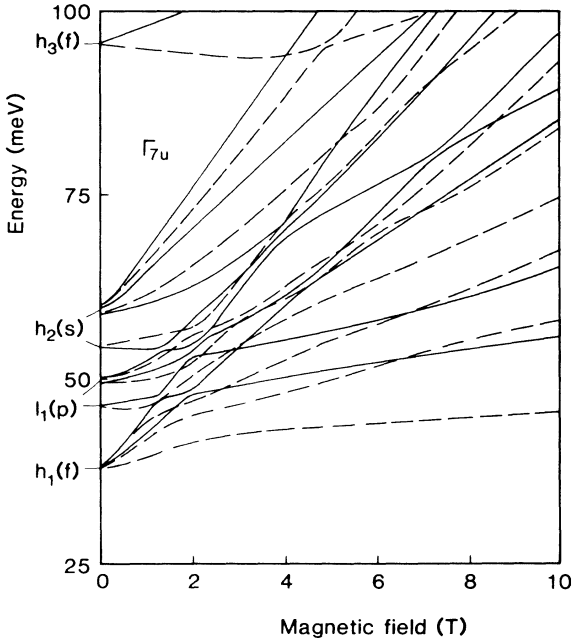

FIG. 19. Γ_{7u} exciton energies of a 100 Å, [001] $GaAs/Al_{0.3}Ga_{0.7}As$ quantum well as a function of magnetic field. The solid (dashed) lines denote association of the s-type envelope function components with $M'=-\frac{3}{2}$ ($M'=\frac{3}{2}$).

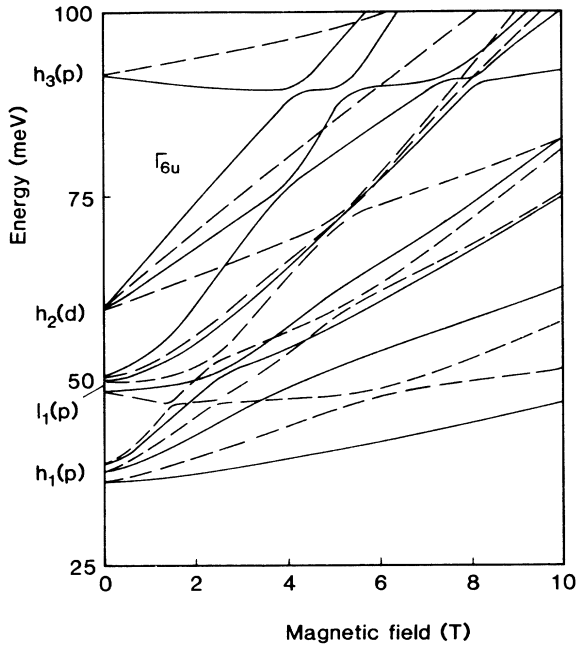

FIG. 20. Γ_{6u} exciton energies of a 100 Å, [001] $GaAs/Al_{0.3}Ga_{0.7}As$ quantum well as a function of magnetic field. The solid (dashed) lines denote association of the s-type envelope function components with $M'=-\frac{1}{2}$ ($M'=\frac{1}{2}$).

that at higher fields $h_1(3d)$ is an excited state for both spin directions, which finally gains oscillator strength again due to mixing with $l_1(2s)$.

Magnetoexciton spectra of quantum wells contain a wealth of information compared to bulk systems. Indeed a plethora of lines are observable in high-resolution exci-

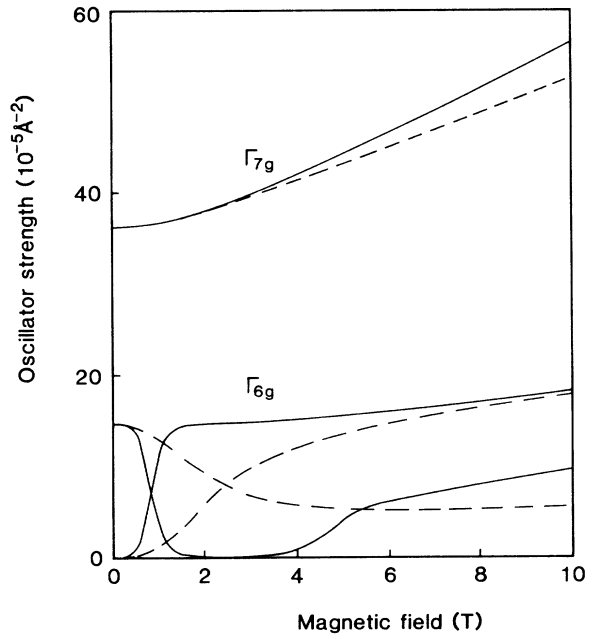

FIG. 21. Oscillator strengths of the low-energy exciton transitions in Figs. 17 and 18 as a function of magnetic field and light polarization (Faraday configuration).

tation spectra.[83] A detailed comparison with the present theory is in preparation.

V. CONCLUSIONS

We have shown that the inhomogeneous two-body problem of excitons in semiconductor quantum wells can be solved with explicit incorporation of the complicated valence-band structure. In this paper and in previous publications we have illustrated the effect of well width, barrier height, crystal direction, external pressure, and electric and magnetic fields on exciton energies and oscillator strengths. The ground states can be calculated with a numerical accuracy of better than 0.1 meV, at least for well widths larger than 50 Å and magnetic fields smaller than 10 T. Most experimental results are explained well by the present model. A discrepancy between calculated and measured ground-state binding energies of $\simeq 1-1.5$ meV remains, which could indicate the need to go beyond the effective-mass approximation. A better treatment of excitonic continuum states and Fano resonances at zero magnetic fields and an improved basis set for states with high quantum numbers in magnetic fields remain desirable. The theory of excitons in genuine superlattices and very narrow and type-II quantum wells[84–86] beyond simple two-band models[87–89] is a challenge for the future.

Note added in proof. Reynolds *et al.* [Phys. Rev. B **37**, 3117 (1988)] recently observed a $3s$ exciton in a wide quantum well. Matsuura [Phys. Rev. B **37**, 6977 (1988)] derived polaron corrections on the exciton binding energies of about 0.1 meV and confirmed our doubts about the results of Ref. 82. Hayakawa *et al.* [Phys. Rev. B **38**, 1526 (1988)] measured term splittings of heavy-hole excitons in [111] quantum wells which were interpreted as an increase of the binding energy of 10% compared to [001] quantum wells. The present theory, on the other hand, predicts a small decrease. We cannot offer an explanation for this discrepancy.

ACKNOWLEDGMENTS

One of the authors (G.E.W.B.) gratefully acknowledges the support as well as constructive criticism of Professor M. F. H. Schuurmans. He would also like to thank Dr. R. Eppenga and Dr. L. Molenkamp for helpful discussions. This work has been supported in part by the Japan Society for the Promotion of Science and by the Grants-in-Aid for Fundamental Scientific Research and Special Distinguished Research from the Ministry of Education of Japan.

APPENDIX: COULOMB MATRIX ELEMENTS

We have to calculate

$$\int dz_e \int dz_h \int d\rho \zeta_i^c(z_e)^* \zeta_j^v(z_h)^* R_{nm}(\rho)^* \times \frac{1}{|\mathbf{r}_e-\mathbf{r}_h|} \zeta_{i'}^c(z_e)\zeta_{j'}^v(z_h)R_{n'm'}(\rho) . \quad \text{(A1)}$$

The integration in the plane of the well is separable from that normal to the well by expressing the Coulomb interaction in terms of the Fourier integral:

$$\frac{1}{|\mathbf{r}_e-\mathbf{r}_h|}=\int\frac{d\mathbf{q}}{2\pi}\frac{1}{q}e^{-q|z_e-z_h|}e^{i\mathbf{q}\cdot\boldsymbol{\rho}}. \tag{A2}$$

The Coulomb interaction is seen to be diagonal in the angular momentum quantum numbers (n,m) by substituting (A1) into (A2) and carrying out the angular integrals. The radial integrals are of the type (N integer)

$$\int d\rho\,\rho^N J_0(\rho q)e^{-\rho/a}, \tag{A3}$$

where $J_0(\rho q)$ is the zero-order Bessel function. Equation (A3) is readily calculated analytically. The integrals over the subband wave functions can be decomposed into a sum of integrals of the type

$$\int_{\pm d_1/2}^{\pm d_2/2}dz_e\int_{\pm d_1/2}^{\pm d_2/2}dz_h e^{\kappa_1^* z_e}e^{\kappa_2^* z_h}e^{-q|z_e-z_h|}e^{\kappa_3 z_e}e^{\kappa_4 z_h}, \tag{A4}$$

where the κ's may be real or imaginary and the integral bounds are determined by the width of the quantum well and the distance to the outer infinite potential barriers which have been introduced to avoid continuum subband states. Equation (A4) is most easily evaluated by using the relation

$$e^{-q|z_e-z_h|}=\int\frac{dt}{\pi}\frac{q}{q^2+t^2}e^{it(z_e-z_h)}. \tag{A5}$$

The z integrals are then easily carried out, while the t integral is evaluated by contour integration. The remaining one-dimensional integrals over the Fourier components q are complicated but well behaved and can be computed numerically with arbitrary precision.

[1]R. Dingle, in *Festkörperprobleme XV (Advances in Solid State Physics)*, edited by H. J. Queisser (Vieweg, Braunschweig, 1975).

[2]R. C. Miller, D. A. Kleinman, W. T. Tsang, and A. C. Gossard, Phys. Rev. B **22**, 1134 (1981).

[3]Y. Masumoto, M. Mitsuura, S. Tarucha, and H. Okamoto, Phys. Rev. B **32**, 4275 (1985).

[4]W. T. Masselink, P. J. Pearah, J. Klem, C. K. Peng, H. Morkoc, G. D. Sanders, and Y. C. Chang, Phys. Rev. B **32**, 8027 (1985).

[5]R. C. Miller, A. C. Gossard, G. D. Sanders, Y.-C. Chang, and J. N. Schulman, Phys. Rev. B **32**, 8452 (1985).

[6]P. Dawson, K. J. Moore, G. Duggan, H. I. Ralph, and C. T. Foxon, Phys. Rev. B **34**, 6007 (1986).

[7]K. J. Moore, P. Dawson, and C. T. Foxon, Phys. Rev. B **34**, 6022 (1986).

[8]J. C. Maan, G. Belle, A. Fasolino, M. Altarelli, and K. Ploog, Phys. Rev. B **30**, 2253 (1984).

[9]N. Miura, Y. Iwasa, S. Tarucha, and H. Okamoto, in *Proceedings of the 17th International Conference on the Physics of Semiconductors, San Francisco, 1984,* edited by J. D. Chadi and W. A. Harrison (Springer, New York, 1985).

[10]W. Ossau, B. Jäkel, E. Bangert, G. Landwehr, and G. Weimann, Surf. Sci. **174**, 188 (1986).

[11]M. Bugajski, W. Kuszko, and K. Reginski, Solid State Commun. **60**, 669 (1986).

[12]D. C. Rogers, J. Singleton, R. J. Nicholas, C. T. Foxon, and K. Woodbridge, Phys. Rev. B **34**, 4002 (1986).

[13]W. Ossau, B. Jäkel, and E. Bangert, in *High Magnetic Fields in Semiconductor Physics,* edited by G. Landwehr (Springer, Berlin, 1987).

[14]W. Ossau, B. Jäkel, E. Bangert, and G. Weimann, in *The Basic Properties of Impurity States in Superlattice Semiconductors,* edited by C. Y. Fong (Plenum, New York, 1988).

[15]A. S. Plaut, J. Singleton, R. J. Nicholas, R. T. Harley, S. P. Andrews, and C. T. Foxon, Phys. Rev. B (to be published).

[16]D. A. B. Miller, D. S. Chemla, T. C. Damen, A. C. Gossard, W. Wiegmann, T. H. Wood, and C. A. Burrus, Phys. Rev. B **32**, 1043 (1985).

[17]L. Viña, R. T. Collins, E. E. Mendez, and W. I. Wang, Phys. Rev. B **33**, 5939 (1986).

[18]R. T. Collins, L. Viña, W. I. Wang, L. L. Chang, L. Esaki, K. von Klitzing, and K. Ploog, Phys. Rev. B **36**, 1531 (1987).

[19]L. Viña, R. T. Collins, E. E. Mendez, and W. I. Wang, Phys. Rev. Lett. **58**, 832 (1987); **59**, 602 (1987).

[20]L. Viña, E. E. Mendez, W. I. Wang, L. L. Chang, and L. Esaki, J. Phys. C **20**, 2803 (1987).

[21]L. Viña, Surf. Sci. **196**, 569 (1988).

[22]L. Viña, G. E. W. Bauer, M. Potemski, J. C. Maan, E. E. Mendez, and W. I. Wang (unpublished).

[23]C. Jagannath, E. S. Koteles, J. Lee, Y. J. Chen, B. S. Elman, and J. Y. Chi, Phys. Rev. B **34**, 7027 (1986).

[24]E. S. Koteles, C. Jagannath, J. Lee, Y. J. Chen, B. S. Elman, and J. Y. Chi, in *Proceedings of the 18th International Conference on the Physics of Semiconductors, Stokholm, 1986,* edited by O. Engström (World Scientific, Singapore, 1987).

[25]L. W. Molenkamp, G. E. W. Bauer, R. Eppenga, and C. T. Foxon, Phys. Rev. B **38**, 6147 (1988).

[26]D. Fröhlich, R. Wille, W. Schlapp, and G. Weimann, Proceedings of the 19th International Conference on the Physics of Semiconductors, Warsaw, 1988, edited by J. Kossut (unpublished).

[27]P. Lefebvre, B. Gil, P. Lascaray, H. Mathieu, D. Bimberg, T. Fukunaga, and H. Nakashima, Phys. Rev. B **37**, 4171 (1988).

[28]E. S. Koteles and J. Y. Chi, Phys. Rev. B **37**, 6332 (1988).

[29]H. I. Ralph, Solid State Commun. **3**, 303 (1965).

[30]M. Shinada and S. Sugano, J. Phys. Soc. Jpn. **10**, 1936 (1966).

[31]G. Bastard, E. E. Mendez, L. L. Chang, and L. Esaki, Phys. Rev. B **26**, 1974 (1982).

[32]Y. Shinozuka and M. Matsuura, Phys. Rev. B **28**, 4878 (1983); **29**, 3717 (E) (1984).

[33]R. L. Greene, K. K. Bajaj, and D. E. Phelps, Phys. Rev. B **29**, 1807 (1984).

[34]T. F. Jiang, Solid State Commun. **50**, 589 (1984).

[35]C. Priester, G. Allan, and M. Lannoo, Phys. Rev. B **30**, 7302 (1984).

[36]O. Akimoto and H. Hasegawa, J. Phys. Soc. Jpn. **22**, 181 (1967).

[37]M. Shinada and K. Tanaka, J. Phys. Soc. Jpn. **29**, 1258 (1970).

[38]R. L. Greene and K. K. Bajaj, Phys. Rev. B **31**, 6498 (1985).

[39]A. H. MacDonald and D. S. Ritchie, Phys. Rev. B **33**, 8336 (1986).

[40]G. Duggan, Phys. Rev. B **37**, 2759 (1988).
[41]F. L. Lederman and J. D. Dow, Phys. Rev. B **13**, 1633 (1976).
[42]J. A. Brum and G. Bastard, Phys. Rev. B **31**, 3893 (1985).
[43]M. Matsuura and T. Kamizato, Phys. Rev. B **33**, 8385 (1986).
[44]M. Altarelli, U. Ekenberg, and A. Fasolino, Phys. Rev. B **28**, 4878 (1983).
[45]T. Ando, J. Phys. Soc. Jpn. **54**, 1528 (1985).
[46]M. Altarelli and N. O. Lipari, Phys. Rev. B **7**, 3798 (1973).
[47]K. Cho, S. Suga, W. Dreybrodt, and F. Willmann, Phys. Rev. B **11**, 1512 (1975).
[48]M. Altarelli and N. O. Lipari, Phys. Rev. B **9**, 1733 (1974).
[49]N. O. Lipari and M. Altarelli, Solid State Commun. **33**, 47 (1980).
[50]Ch. Neumann, A. Nöthe, and N. O. Lipari, Phys. Rev. B **37**, 922 (1988).
[51]G. D. Sanders and Y. C. Chang, Phys. Rev. B **32**, 5517 (1985); **35**, 1300 (1987).
[52]D. A. Broido and L. J. Sham, Phys. Rev. B **34**, 3917 (1986).
[53]K. S. Chan, J. Phys. C **19**, L125 (1986).
[54]U. Ekenberg and M. Altarelli, Phys. Rev. B **35**, 7585 (1987).
[55]B. Zhu and K. Huang, Phys. Rev. B **36**, 8102 (1987).
[56]B. Zhu, Phys. Rev. B **37**, 4689 (1988).
[57]L. C. Andreani and A. Pasquarello, Europhys. Lett. **6**, 259 (1988).
[58]G. D. Sanders and Y. C. Chang, Phys. Rev. B **32**, 4282 (1985).
[59]G. D. Sanders and K. K. Bajaj, Phys. Rev. B **35**, 2301 (1987); **36**, 4849 (1987).
[60]T. Hiroshima, Phys. Rev. B **36**, 4518 (1987).
[61]S. R. Eric Yang and L. J. Sham, Phys. Rev. Lett. **58**, 2598 (1987).
[62]F. Ancilotto, A. Fasolino, and J. C. Maan, J. Superlatt. Microstruct. **3**, 187 (1987).
[63]B. Jäkel, W. Ossau, and E. Bangert (unpublished).
[64]W. T. Masselink, Y.-C. Chang, and H. Morkoc, Phys. Rev. B **32**, 5190 (1985).
[65]J. M. Luttinger, Phys. Rev. **102**, 1030 (1956).
[66]G. E. W. Bauer and T. Ando, *Proceedings of the 18th International Conference on the Physics of Semiconductors, Stokholm, 1986,* edited by O. Engström (World Scientific, Singapore, 1987).
[67]G. E. W. Bauer and T. Ando, Phys. Rev. Lett. **50**, 601 (1987).
[68]G. E. W. Bauer and T. Ando, J. Phys. (Paris) Colloq. **48**, C5-215 (1987).
[69]G. E. W. Bauer and T. Ando, Phys. Rev. B **37**, 3130 (1988).
[70]G. E. W. Bauer, in *Application of High Magnetic Fields in Semiconductor Physics,* edited by G. Landwehr (Springer, Berlin, in press).
[71]G. Dresselhaus, J. Phys. Chem. Solids **1**, 14 (1956).
[72]J. O. Dimmock, in *Semiconductors and Semimetals,* edited by R. K. Willardson and A. C. Beer (Academic, New York, 1972), Vol. 9.
[73]H. Akera, S. Wakahara, and T. Ando, Surf. Sci. **196**, 694 (1988).
[74]M. Altarelli, Phys. Rev. B **28**, 842 (1983).
[75]M. F. H. Schuurmans and G. W. t'Hooft, Phys. Rev. B **31**, 8041 (1985).
[76]R. Eppenga, M. F. H. Schuurmans, and S. Colak, Phys. Rev. B **36**, 1554 (1987).
[77]K. Suzuki and J. C. Hensel, Phys. Rev. B **9**, 4184 (1974).
[78]K. Cho, Phys. Rev. B **14**, 4463 (1976).
[79]J. N. Schulman and Y. C. Chang, Phys. Rev. B **31**, 2056 (1985).
[80]C. Hermann and C. Weisbuch, in *Optical Orientation,* edited by F. Meier and B. P. Zakharchenya (Elseviers, Amsterdam, 1984).
[81]L. W. Molenkamp, R. Eppenga, G. W. t'Hooft, P. Dawson, C. T. Foxon, and K. J. Moore Phys. Rev. B **38**, 4314 (1988).
[82]M. H. Degani and O. Hipolito, Phys. Rev. B **35**, 4507 (1987).
[83]L. Viña, G. E. W. Bauer, M. Potemski, J. C. Maan, E. E. Mendez, and W. I. Wang (unpublished).
[84]K. J. Moore, P. Dawson, and C. T. Foxon, Phys. Rev. B **38**, 3386 (1988).
[85]K. J. Moore, G. Duggan, P. Dawson, and C. T. Foxon, Phys. Rev. B **38**, 5535 (1988).
[86]H. van Kesteren, E. C. Cosman, F. J. A. M. Greidanus, P. Dawson, K. J. Moore, and C. T. Foxon, Phys. Rev. Lett. **61**, 129 (1988).
[87]G. Duggan and H. I. Ralph, Phys. Rev. B **35**, 4152 (1987).
[88]H. Chu and Y.-C. Chang, Phys. Rev. B **36**, 2946 (1987).
[89]B. Rejaei Salmassi and G. E. W. Bauer (unpublished).